INTERNATIONAL SOCIETY FOR
SOIL MECHANICS AND
GEOTECHNICAL ENGINEERING

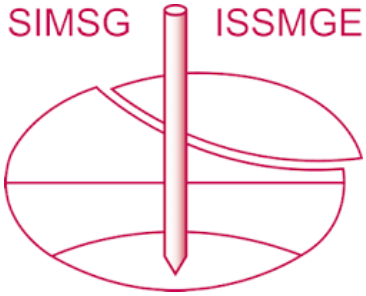

This paper was downloaded from the Online Library of the International Society for Soil Mechanics and Geotechnical Engineering (ISSMGE). The library is available here:

https://www.issmge.org/publications/online-library

This is an open-access database that archives thousands of papers published under the Auspices of the ISSMGE and maintained by the Innovation and Development Committee of ISSMGE.

The paper was published in the proceedings of the 7th International Conference on Earthquake Geotechnical Engineering and was edited by Francesco Silvestri, Nicola Moraci and Susanna Antonielli. The conference was held in Rome, Italy, 17 – 20 June 2019.

Earthquake Geotechnical Engineering for Protection and Development of Environment and Constructions – Silvestri & Moraci (Eds)
© 2019 Associazione Geotecnica Italiana, Rome, Italy, ISBN 978-0-367-14328-2

Effects of hyperbolic hardening parameters on seismic response of high rise buildings considering soil-structure interaction

N. Yeganeh & B. Fatahi
School of Civil and Environmental Engineering, University of Technology Sydney (UTS), Sydney, NSW, Australia

S. Mirlatifi
John Holland, Sydney, NSW, Australia

ABSTRACT: Seismic soil-structure interaction is referred to the process wherein the soil dynamic response is influenced by the structure motion whilst the latter is also affected by the soil motion. To assess the seismic response of the soil-structure systems, selecting the appropriate soil model parameters is of great importance and the predictions can be significantly impacted if the simply assumptive parameters, presented in the literature, are employed. In this study, the strain hardening soil constitutive model, named "hyperbolic hardening with hysteretic damping", was employed in the 3D coupled soil-structure interaction numerical simulations using FLAC3D. Utilizing the numerical simulations, the impact of the choice of the soil model parameters, in the range, recommended in the literature, on the seismic response of a moment-resisting building was assessed. It was concluded that the relation between the hyperbolaand Mohr-Coulomb failurecriterion hasa major contribution to the prediction of the seismic response of a building considering the soil-structure interaction.

1 INTRODUCTION

The recent research studies on the seismic Soil-Structure Interaction (SSI) (e.g. Gazetas 2015, Nguyen et al. 2016, Nguyen et al. 2017, Fatahi et al. 2018, Xu & Fatahi 2019), have demonstrated the importance of SSI in the geotechnical earthquake engineering applications. Lade (2005) pointed out that the predictions of the structures response, subjected to the external loading, very much depend on the stress-strain relationship, known as the constitutive model. Indeed, there are numerous plasticity-based soil constitutive models in the literature, being frequently employed in the SSI numerical simulations (e.g. Castaldo & De Iuliis 2014, Yeganeh et al. 2015), whereas the engineers might need to use some assumptive values for some of the parameters based on the reported ranges in the literature for the various soils. It has been realized that assessing the extent to which the choice of such assumptive parameters can affect the seismic response of the superstructures has not been fully scrutinized. In this study, the Hyperbolic Hardening with Hysteretic Damping (H2-HD) model was cherry-picked among the advanced hardening plasticity-based soil constitutive models. In order to investigate the above-mentioned effects, FLAC3D software and its internal programming language, named "FISH", were utilized so as to numerically analyze a fully coupled soil-structure system in the time domain.

2 ADOPTED SOIL-STRUCTURE INTERACTIONNUMERICAL MODEL

A 20-story (60 m height), 3-span (12 m length) reinforced concrete moment-resisting building was analyzed and designed using SAP2000 considering the relevant Australian codes and in line with the constructability and norms. The properties of the Grade-32 concrete material, adopted in the building (i.e. the columns, beams, and 0.25-m slabs) and foundation, are as follows: (i) modulus

of elasticity, equal to 30.1 GPa; (ii) Poisson's ratio of 0.2; (iii) mass density of 2400 kg/m^3; and (iv) specified compressive strength = 32 MPa. The possibility of forming the plastic hinges was considered in the rectangular columns and beams by specifying the limiting plastic moment (M_p) based on and the geometries of the structural elements. Consequently, the structural elements behaved elastically until breaching the defined plastic moment. If the limiting plastic moment was reached, the section could deform without inducing any additional resistance. The adopted sizes of the columns and beams were 0.85 m×0.85 m and 0.70 m×0.70 m till the fifth story, respectively, and above which the dimensions were reduced by 0.05 m every five floors. Moreover, according to ACI318 (2014), the cracked section properties for the reinforced concrete components were employed by diminishing the stiffness of the columns (to 0.70 I_g), beams (to 0.35 I_g), and slabs (to 0.25 I_g), considering I_g as the moment of inertia associated with an uncracked section. Besides, a damping ratio of 5% was adopted to consider the vibration dissipation of the superstructure and foundation. The designed mat foundation had a thickness of 1 m and a width of 14 m while the building total width was 12 m. The Meyerhof method (Bowles 1996) showed the satisfaction of the minimum required factor of safety (FOS) of 3 for the bearing capacity of the adopted mat foundation, subjected to the building weight.

The adopted plan dimensions of the soil medium, shown in Figure 1, were 70 m×70 m, satisfying the minimum requirement, being five times the width of the existing building (Rayhani & El Naggar 2008). The convergence analysis was also performed on the zone sizes for rationally reducing the seismic analysis time without impacting the predictions. In addition, the free field boundary conditions were applied to the lateral boundaries of the soil deposit to simulate the seismic motions, propagating along the edges of the numerical model. Furthermore, the viscous dashpots, coupled with the said free field boundaries, were utilized so as to absorb the boundary wave reflections. It should be highlighted that the fully fixed base and horizontally fixed side boundaries were adopted in the static analysis, subjected to the gravity loading, prior to applying the earthquake excitation. Furthermore, the seismic bedrock at the model base was considered as a rigid base due to the significant impedance difference between the hard rock and soil deposit. Further, the 30-m thickness of the soil deposit was selected since Maheswari et al. (2010) reported that the potential amplification/attenuation of a site during the ground shaking could be predicted throughout the properties of the top 30 m of the soil. The baseline-corrected near-field excitation of the 1994 Northridge earthquake (USA), portrayed in Figure 2, was imposed upon the bedrock level to carry out the time-history analysis. The severity of the damage associated with the near-field ground motions, e.g. the 1994 Northridge earthquake, was outlined by Attalla et al. (1998). In this study, the mat foundation was modeled using the solid zones, capturing the shear deformations of the foundation under the applied loads. Last but foremost, the possible separation, gapping, and/or sliding at the interface between the concrete mat foundation and soil, were captured by means of the interface element, represented by the springs and sliders. The normal and shear spring stiffnesses were set to ten times the stiffness of the neighboring zone (Itasca 2012), while the Mohr-Coulomb yield criterion was assigned to the sliders.

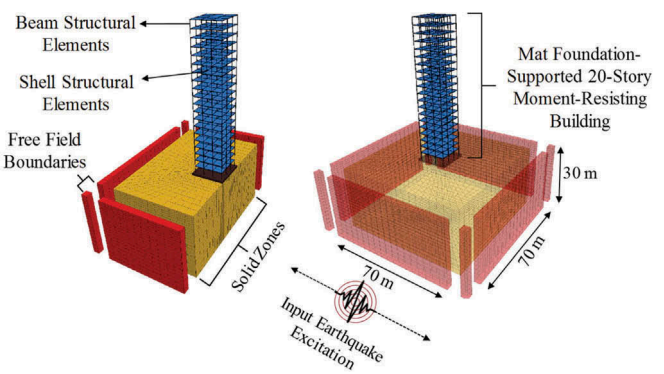

Figure 1. Adopted soil-structure system via direct one-step approach in FLAC3D.

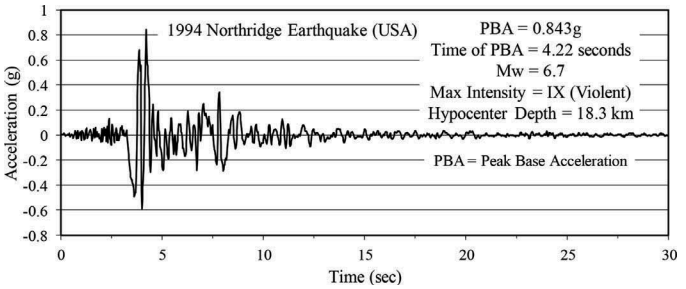

Figure 2. Adopted earthquake accelerogram of 1994 Northridge Earthquake as input base motion.

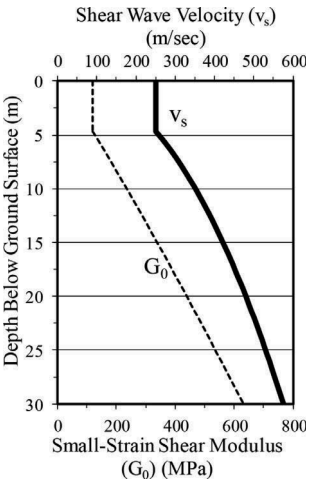

Figure 3. Adopted shear wave velocity and small-strain shear modulus profiles.

3 ADOPTED SOIL CONSTITUTIVE MODEL

The adopted Hyperbolic Hardening with Hysteretic Damping soil model, called hereinafter H2-HD, inspired by the UBCSAND model (Puebla 1999), captured the shear hardening, volumetric hardening, and Mohr-Coulomb failure envelope. The detailed description of the H2-HD soil constitutive model was reported by Yeganeh & Fatahi (2019). In addition to the nonlinear elasticity considering the Hook's law in the incremental manner, the two-variable hysteretic damping algorithm, stemming from the small-strain nonlinearity, was employed in this study (see Table 2).

The shear hardening law, revised from the well-known hyperbolic model, established by Duncan et al. (1970), offered the possibility of expressing the hyperbolic behavior via the relation between the developed stress ratio (*SR*) and plastic shear strain (γ_p), given in Equation 1. *SR* was defined as the sine of a mobilized friction angle (φ_{mob}), whose ultimate value was the failure effective friction angle (φ'_f).

$$d(SR) = d(\sin\varphi_{mob}) = \frac{G_p}{p'} d(\gamma p) = \frac{G_p^i}{p'} (1 - R_f \frac{\sin\varphi_{mob}}{\sin\varphi'_f})^2 d(\gamma p) = \frac{\beta G_e}{p'} (1 - R_f \frac{\sin\varphi_{mob}}{\sin\varphi'_f})^2 d(\gamma p) \quad (1)$$

where G_p^i = initial tangent plastic shear modulus at very low stress ratio level (*SR* near 0); β = elastic-plastic coupling coefficient; G_e = elastic shear modulus, whose initial distribution (i.e.G_0), consistent with shear wave velocity (v_s) profile, is displayed in Figure 3; and R_f = failure ratio.

Equation 2 formulates the shear yield locus, corresponding to a constant stress ratio and the mobilized intercept ($c'(\tan\varphi_{mob})(\tan\varphi'_f)^{-1}$, where c' = ultimate effective cohesion) in the p'-q space. The compression yield surface (f_c) was a straight line, perpendicular to the mean effective stress

axis (p') and independent of the deviatoric stress (q). In the H2-HD model, the associated and non-associated flow rules were adopted for the volumetric and shear responses, in the order given.

$$f_s = p'\left(\frac{6\sin\varphi_{mob}}{3-\sin\varphi_{mob}}\right) + c'\left(\frac{\tan\varphi_{mob}}{\tan\varphi_f'}\right)\left(\frac{6\cos\varphi_{mob}}{3-\sin\varphi_{mob}}\right) - q \quad (2)$$

By means of a cap hardening power law, the nonlinear volumetric behaviorwas reproduced. The cap pressure (P_c) in Equation 3, defined the size of the compression yield surface in compliance with the irrecoverable volumetric strain (ε_p). Note that the in-situ stress state wassimulated based on the coefficient of lateral earth pressure at rest for the overconsolidated soil deposit ($K_{0\,(oc)}$). As the analysis was up and running, the elastic tangent bulk (K_e) and shear (G_e) moduli were evolving as a function of P_c and p', as given in Equation 4 and Equation 5, respectively. Simply put, the stress-dependent elastic stiffness was taken into account in the H2-HD soil model.

$$p_c = p_{ref}(0.12\varepsilon_p(\frac{K_{ref}}{p_{ref}}))^{(1/0.1)} \quad (3)$$

$$K_e = K_{ref}^{e-p}(\frac{P_c}{P_{ref}})^{0.9} \quad (4)$$

$$G_e = G_{ref}(\frac{p'}{P_{ref}})^{0.9} \quad (5)$$

where $K^{e\text{-}p}{}_{ref}$= isotropic elasto-plastic bulk modulus at reference effective pressure (p_{ref}); and G_{ref} = elastic tangent shear modulus at p_{ref}. Theoretically, p_{ref} could be any value so long as K_{ref} and G_{ref} are given correspondingly (Sadat et al. 2018).

4 ADOPTED HYPERBOLIC HARDENING PARAMETERS

In the adopted elasto-plastic soil constitutive model, the failure ratio (R_f) and elastic-plastic coupling coefficient (β) were the key parameters, influencing the stress increment-strain increment relationship, affecting the induced plastic shear strains significantly. Through the adopted formulations, the failure ratio could affect not only the soil strength but also the soil stiffness. In the adopted soil model, the failure ratio linked the hyperbolic asymptote, i.e. the ultimate strength (SR_{ult}), to the Mohr-Coulomb failure envelope (i.e. SR_f) via Equation 6. In addition, the decremental slope of the employed hyperbola (G_p in Equation 1) was altered by assigning the different values to the failure ratio, i.e.0.7, 0.8, and 0.9, denoting the changes in the soil stiffness. It is to be noted that R_f should be always less than 1.0 and greater than 0.7 (see Wong & Broms 1989).

$$SR_{ult} = (R_f)^{-1}SR_f = (R_f)^{-1}\sin(\varphi_f') \quad (6)$$

While R_f prevented the overprediction of the ultimate shear strength in the conducted numerical simulations, the dimensionless elastic-plastic coupling coefficient supervised the initial tangent slope of the hyperbola at the very low stress ratios. Said otherwise, the initial tangent plastic shear modulus (G^i_p) in Equation 1 was overseen by β. Allocating three values, i.e. 0.10, 0.20, and 0.35, to β was in line with the fact that β, usually less than 1 (Byrne et al. 2003, Sadat et al. 2018), practically depends on the relative density (D_r) as per Equation 7, recommended by Byrne et al. (2004). The adopted relative density for the soil of interest was assumed to be 48% (±8%) to cover the common range for a medium dense soil deposit, reported by Budhu (2010). The summary of the adopted scenarios for the various R_f and β parameters is presented in Table 1. The effects of the adopted values for the failure ratio and elastic-plastic coupling coefficient on the performance of the H2-HD soil constitutive model in the space of SR-γ_p are graphically illustrated in Figure 4. The rest of the parameters attributed to the H2-HD model are tabulated in Table 2.

$$\beta \approx 3.7(D_r)^4 \quad (7)$$

Table 1. Developed numerical models based on adopted R_f and β.

Case ID	I	II	III	IV	V
R_f	0.70	0.80	0.90	0.70	0.70
β	0.35	0.35	0.35	0.20	0.10

Table 2. Adopted soil properties for considered soil deposit.

Soil parameter	Symbol	Value	Unit
Density	ρ	1900	kg/m^3
Poisson's ratio	υ	0.3	-
Failure effective friction angle	φ'_f	29	°
Dilatancy	ψ	0	°
Ultimate effective cohesion	c'	20	kPa
Stress ratio at failure	SR_f	0.48	-
Shear wave velocity @depth of 6 m	v_s	280	m/s
Small-strain shear modulus @depth of 6 m	G_0	149	MPa
Initial elastic tangent bulk modulus @depth of 6 m	K_{ei}	323	MPa
Overconsolidated K_0 coefficient @depth of 6 m	$K_{0(oc)}$	0.88	-
Overconsolidation ratio @depth of 6 m	OCR	3.1	-
Isotropic elasto-plastic bulk modulus @depth of 6 m	$K^{e\text{-}p}{}_{ref}$	428	MPa
P_{ref}-related elastic tangent shear modulus @depth of 6 m	G_{ref}	196	MPa
Initial cap pressure @depth of 6 m	P_{ci}	310	MPa
Hysteretic damping parameters (Itasca 2012)	L_1&L_2	-3.325&0.823	-

* Reference effective pressure (P_{ref}) at depth of 6 m equaled atmospheric pressure (P_{atm}), i.e.100 kPa.

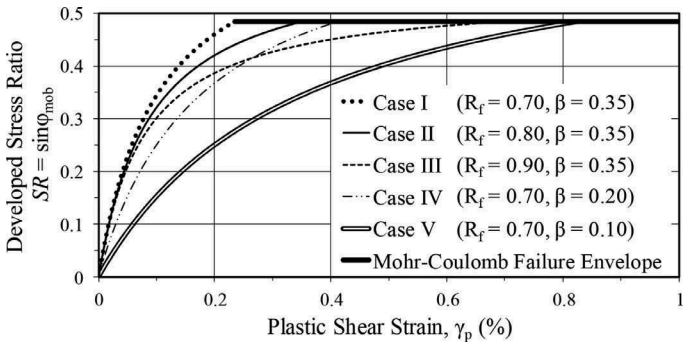

Figure 4. Implemented hyperbolic hardening relationships at depth of 6 m for developed numerical cases.

5 RESULTS AND DISCUSSIONS

Figure 5 displays the response spectra of the motions at the bedrock and ground surface through the Duhamel integral method, adopting 5% damping ratio. As is evident in Figure 5, some level of attenuation occurred almost for all the considered cases owing to the contribution of the hardening plasticity and perfect plasticity-induced damping as well as the hysteretic damping feature. The estimated effective period range of the soil-structure system from the second mode to the fundamental/first mode was 0.48-1.90 seconds. Figure 5 reveals that decreasing the failure ratio (R_f) or increasing the elastic-plastic coupling coefficient (β) led to augmenting the inertial forces in the superstructure during the earthquake since the trend of Case I sat atop the others in the aforesaid effective period range.

The maximum story shear forces are shown in Figure 6, determined by taking the summation of all the columns shear forces on the same level once reaching the utmost during the excitation. Referring to Figure 6, about 30% diminishment in the story shear force on the 6th story from

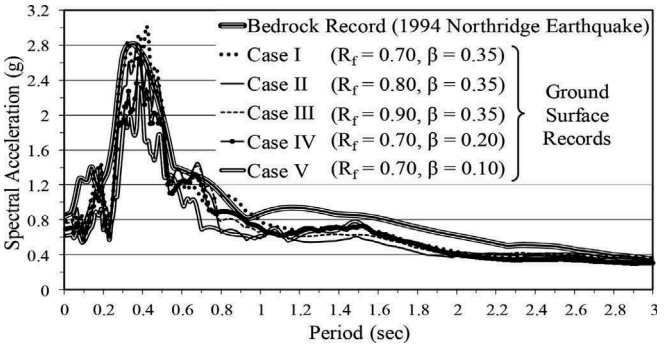

Figure 5. Response spectra of bedrock record and ground motions.

Case I to Case V was observed. Indeed, the effect of β on the structural demand outweighed that of R_f. Reducing the elastic-plastic coupling coefficient, whilst keeping R_f constant (i.e. comparing Cases I, IV, and V), induced the 15% reduction in the base shear, whereas the corresponding drop due to the changes in R_f was about 4%(i.e. comparing Cases I, II, and III). The reason was that increasing β abated the hardening plasticity-induced damping and hysteretic damping much more than decreasing R_f owing to shortening the hyperbolic path towards the Mohr-Coulomb failure envelope, referring back to Figure 4.

As sketched in Figure 7, the foundation rocking rotations were ascended by the rise in the structural forces, as previously reported in Figure 6. The lower the R_f value (e.g. Case I), the more contribution of the brittle manner to the soil behavior and thus giving rise to the soil perfect plasticity status at the low plastic shear strains. For instance, the permanent rotation of the foundation slab was 0.50 degrees for Case I whereas the corresponding value in Case V declined by over 50% to 0.24 degrees. When the Mohr-Coulomb failure envelope was reached at the large plastic shear strains (see Figure 4), the lowest values of the transient foundation rocking were observed. It should be noted that the said values for Case III and Case V were 0.50 degrees and 0.39 degrees, consecutively.

The lateral deflections of the adopted 20-story building, stemming from the combination of the structural distortion and foundation rocking, reported in Figure 8, were obtained once the roof-top displacement reached its utmost during the seismic excitation. In this study, the foundation rocking contributed more into the lateral displacement of the building. As displayed in Figure 8, Case I, in agreement with Figures 6-7, underwent the highest lateral displacements, e.g. about 750 mm at the top level (roof), compared to the rest. Sozen (1981) proclaimed that an inter-story drift of 0.5% is acceptable to almost any critic, experienced by Case V, displayed in Figure 8. Nonetheless, the expected percentages of the structural damage according to Equation 8 (Sozen 1981), where δ_{max} = maximum inter-story drift ratio in percentage, were 21%, 18%, and 12% for Case I, Case II, and Case III, respectively.

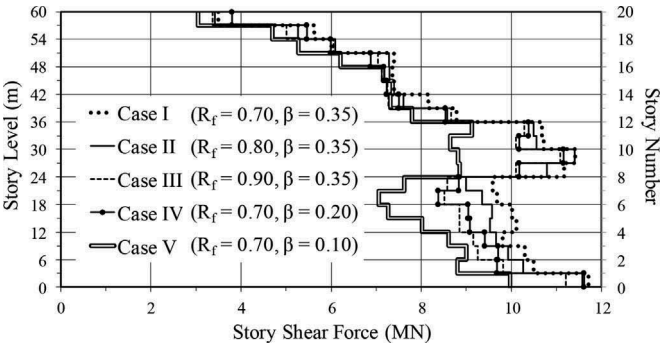

Figure 6. Maximum shear force distributions over height of building under 1994 Northridge earthquake.

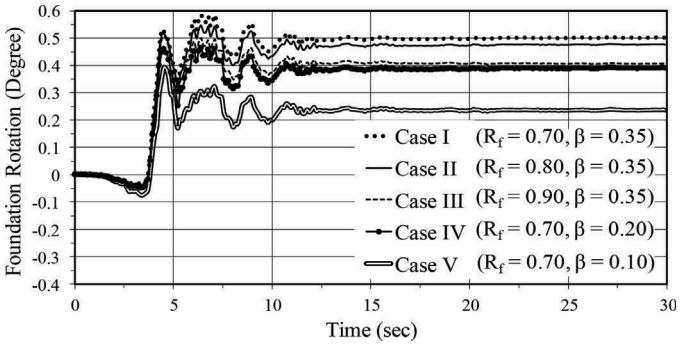

Figure 7. Foundation rocking histories under 1994 Northridge earthquake.

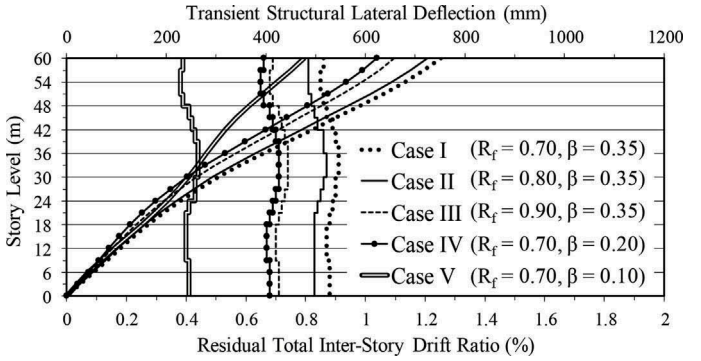

Figure 8. Transient lateral deflections and residual drifts of building under 1994 Northridge earthquake.

$$\%\ \text{of Damage} = 50\delta_{max} - 25 \tag{8}$$

In summary, it could be deduced that estimating the parameters values in a plasticity-based soil model could preclude any potential damage to the soil-structure systems due to the earthquakes or result in the optimized and more cost-effective design.

6 CONCLUSIONS

The key contribution of the current research was investigating the extent to which the choice of the hyperbolic hardening parameters would be capable of impacting the seismic response of the buildings considering SSI. Such parameters, affecting the plastic strain hardening rule, were the failure ratio (R_f) and elastic-plastic coupling coefficient (β) in the Hyperbolic Hardening with Hysteretic Damping (H2-HD) soil constitutive model.A series of 3D fully coupled nonlinear numerical analyses of the soil-structure system was conducted in FLAC3D by adopting the direct method whereby the entire system was analyzed in one attempt during the applied earthquake.

Examining the geotechnical and structural objectives herein, such as the response spectra at the bedrock and ground surface, story shear forces developed in the structure, structural lateral displacements, and inter-story drift ratios, divulged that the initial and decremental slopes of the plastic form of the hyperbola in combination with how soon violating the shear failure envelope could be the culprit of the unsafe design in some cases. In other words, this study demonstrated that the right selection of the parameters in the H2-HD constitutive model (e.g. via the calibration of the model parameters to the laboratory test data, such as the triaxial test results) could result in the safer or even more cost-effective design of the superstructures, subjected to the strong earthquakes.

It is recommended by the current study to the practicing engineers to conduct the laboratory tests so as to obtain the parameters associated with the chosen advanced hardening

plasticity-based soil models since the inaccurate selection of the model parameters based on some general recommendations in the literature could result in the unreliable predictions, jeopardizing the safety or resulting in the significantly overdesigned or expensive construction.

REFERENCES

ACI318, 2014. Building code requirements for structural concrete and commentary. Farmington Hills: American Concrete Institute.

Attalla, M.R. Paret, T.F. & Freeman, S.A. Near-source behavior of buildings under pulse-type earthquakes. In Proceedings of the sixth US National Conference on Earthquake Engineering; Seattle, 31 May - 4 June 1998.

Bowles, L.E. (5th ed.) 1996. Foundation analysis and design. New York: McGraw-hill.

Budhu, M. (3rd ed.) 2010. Soil Mechanics and Foundations. New York: John Wiley & Sons.

Byrne, P.M. Park, S.S. & Beaty, M. Seismic liquefaction: centrifuge and numerical modeling. In Richard Brummer, Patrick Andrieux, Christine Detournay & Roger Hart (ed.), FLAC and numerical modeling in geomechanics; In Proceedings of third International FLAC Symposium, Sudbury, 21-24 October 2003. Lisse: August Aimé Balkema.

Byrne, P.M. Park, S.S. Beaty, M. Sharp, M. Gonzalez, L. & Abdoun, T. 2004. Numerical modeling of liquefaction and comparison with centrifuge tests. Canadian Geotechnical Journal 41(2): 193-211.

Castaldo, P. & De Iuliis, M. 2014. Effects of deep excavation on seismic vulnerability of existing reinforced concrete framed structures. Soil Dynamics and Earthquake Engineering 64: 102-112.

Duncan, J.M. & Chang, C.Y. 1970. Nonlinear analysis of stress and strain in soils. Journal of the Soil Mechanics and Foundations Division 96:1629-1653.

Fatahi, B. Nguyen, Q.V. Xu, R. & Sun, W.J. 2018. Three-dimensional response of neighboring buildings sitting on pile foundations to seismic pounding. International Journal of Geomechanics 18(4): 04018007.

Gazetas, G. 2015. 4th Ishihara lecture: Soil-foundation-structure systems beyond conventional seismic failure thresholds. Soil Dynamics and Earthquake Engineering 68: 23-39.

Itasca, 2012. User's Manual FLAC3D: Fast lagrangian analysis of continua in 3 dimensions (version 5.0.). Minneapolis: Itasca International Inc.

Lade, P.V. 2005. Overview of constitutive models for soils. ASCE Geotechnical Special Publication-Soil Constitutive Models: Evaluation, Selection, and Calibration 128: 1-34.

Maheswari, R.U. Boominathan, A. & Dodagoudar, G.R. 2010. Seismic site classification and site period mapping of Chennai City using geophysical and geotechnical data. Journal of Applied Geophysics 72 (3): 152-168.

Nguyen, Q.V. Fatahi, B. & Hokmabadi, A.S. 2016. The effects of foundation size on the seismic performance of buildings considering the soil-foundation-structure interaction. Structural Engineering and Mechanics 58(6): 1045-1075.

Nguyen, Q.V. Fatahi, B. & Hokmabadi, A.S. 2017. Influence of size and load-bearing mechanism of piles on seismic performance of buildings considering soil-pile-structure interaction. International Journal of Geomechanics 17(7): 04017007.

Puebla, H. 1999. A constitutive model for sand and the analysis of the CanLex Embankments. Doctoral dissertation. Vancouver: University of British Columbia.

Rayhani, M.H. & El Naggar, M.H. 2008. Numerical modeling of seismic response of rigid foundation on soft soil. International Journal of Geomechanics 8(6): 336-346.

Sadat, M.R. Huang, J. Bin-Shafique, S. & Rezaeimalek, S. 2018. Study of the behavior of mechanically stabilized earth (MSE) walls subjected to differential settlements. Geotextiles and Geomembranes 46(1): 77-90.

Sozen, M.A. Review of earthquake response of reinforced concrete buildings with a view to drift control. In OktayErgunay& Mustafa Erdik (ed.), State-of-the-art in earthquake engineering: state-of-the-art panel reports prepared for the occasion of seventh world conference on earthquake engineering; Istanbul, 8-13 September 1981. Ankara: Turkish National Committee on Earthquake Engineering.

Wong, K.S. & Broms, B.B. 1989. Lateral wall deflections of braced excavations in clay. Journal of Geotechnical Engineering 115(6): 853-870.

Xu, R. & Fatahi, B. 2019. Novel application of geosynthetics to reduce residual drifts of mid-rise buildings after earthquakes. Soil Dynamics and Earthquake Engineering 116:331-344.

Yeganeh, N. Bazaz, J.B. & Akhtarpour, A. 2015. Seismic analysis of the soil-structure interaction for a high rise building adjacent to deep excavation. Soil Dynamics and Earthquake Engineering 79: 149-170.

Yeganeh, N. & Fatahi, B. 2019. Effects of choice of soil constitutive model on seismic performance of moment-resisting frames experiencing foundation rocking subjected to near-field earthquakes. Submitted to Soil Dynamics and Earthquake Engineering (Accepted).